Magnetite and magnetite/silver core/shell nanoparticles with diluted magnet-like behavior

Marco Garza-Navarro [a], Alejandro Torres-Castro [a,b,*], Virgilio González [a,b], Ubaldo Ortiz [a,b], Elder De la Rosa [c]

[a] Facultad de Ingeniería Mecánica y Eléctrica, Universidad Autónoma de Nuevo León, Av. Universidad s/n, Cd. Universitaria, San Nicolás de los Garza, Nuevo León 66450, México
[b] Centro de Innovación, Investigación y Desarrollo en Ingeniería y Tecnología, Universidad Autónoma de Nuevo León, Apodaca, Nuevo León 66600, México
[c] Centro de Investigaciones en Óptica, A.P. 1-948, León Gto. 37160, México

ABSTRACT

In the present work is reported the use of the biopolymer chitosan as template for the preparation of magnetite and magnetite/silver core/shell nanoparticles systems, following a two step procedure of magnetite nanoparticles in situ precipitation and subsequent silver ions reduction. The crystalline and morphological characteristics of both magnetite and magnetite/silver core/shell nanoparticles systems were analyzed by high resolution transmission electron microscopy (HRTEM) and nanobeam diffraction patterns (NBD). The results of these studies corroborate the core/shell morphology and the crystalline structure of the magnetite core and the silver shell. Moreover, magnetization temperature dependent, $M(T)$, measurements show an unusual diluted magnetic behavior attributed to the dilution of the magnetic ordering in the magnetite and magnetite/silver core/shell nanoparticles systems.

© 2009 Elsevier Inc. All rights reserved.

1. Introduction

Core/shell nanoparticles have attracted the attention of the scientific community due to their unique physical and chemical properties that suggest potential applications in diverse techno-logical fields such as semiconductor electronics and biomedical industries [1–3]. Specifically, the synthesis of core/shell magnetic nanoparticles deserve particular importance due to their possible applications in magnetic resonance imaging for diagnostic and thermal therapies [4–6], controlled drug targeting delivery [7–8], chemical separator and chemical sensors [9], and high density magnetic recording [10–12]. However, the information about the synthesis of metal-oxide/metal nanoparticles with controllable size is relatively limited. For example, it has been reported that the synthesis of water soluble magnetite/gold nanoparticles enhance biocompatibility and chemical stability by protecting the magnetic core from further oxidation [13,14]. Such properties are very important for biomedical applications. In those works, the synthetic procedure is based on the reduction of Au ions in the presence of previously synthesized and stable magnetite cores.

Nanoparticles with ferromagnetic core coated with antiferro-magnetic or ferrimagnetic shell have been synthesized. These particles are known as bimagnetic [11,12]. The coating of ferromagnetic ordered nanoparticles with ferrimagnetic shell, such as iron oxides maghemite and magnetite, leads to an enhancement on its magnetic properties due to an effective exchange coupling at the core-shell interfacial magnetic moment [10–12]. Moreover, it has been reported that the synthesis of antiferromagnetic ordered shell over ferro-ferrimagnetic nano-particles or vice-versa, induces temperature dependent magnetic ordering beyond superparamagnetic relaxation, leading a shift in the blocking temperature, which tends to reach temperature near to room temperature [15–17].

In addition, one can find literature related to synthetic approaches focused to the development of silver/magnetite core/shell, where colloidal dispersions of silver nanoparticles and ferric ions are used to perform in situ precipitation and subsequent coating of those metal nanoparticles with magnetite shell [18]. It has been reported that the preparation of metal coating metal-oxide core/shell systems, where magnetite nano-particles dispersions was used to perform in situ reduction reaction of silver ions by the addition of glucose as reducing agent [18–20]. However, in spite of according to these approaches it is possible to obtain core/shell nanoparticles of silver/magnetite or vice-versa, it consider the preparation of silver or magnetite

* Corresponding author at: Facultad de Ingeniería Mecánica y Eléctrica, Universidad Autónoma de Nuevo León, Av. Universidad s/n, Cd. Universitaria, San Nicolás de los Garza, Nuevo León 66450, México.
E-mail address: alejandro.torrescs@uanl.edu.mx (A. Torres-Castro).

cores using methods such as microemulsion and polyol, where both particle size and morphology are highly dependent of reactant concentration. It is important to remark that in those methods the re-dispersion of the cores is performed usually in organic dissolvent at diluted concentrations.

Accordingly, the biopolymer chitosan is a promising stabilization media of iron oxide nanoparticles, since it has been reported that is possible to reach iron-oxide/chitosan ratios as high as 4.5 [21]. The chitosan is a polyamine-saccharide which presents a remarkable affinity to form coordination compounds between its amine and hydroxyl fuctional groups and transition metal ions such as Fe(II), Fe(III), Co(II), Cu(II), Ni(II), Pb(II), Cd(II) and Cd(IV) [22–29]. Considering this important feature, it has been possible to synthesize magnetite–chitosan magnetic composites using the co-precipitation method in order to obtain chitosan spheres coated with magnetic nanoparticles [30–32]. Moreover, as has been previously reported, chitosan presents relative permeability to the diffusion of silver ions, which indicates that could be possible the synthesis of magnetite/silver core/shell nanoparticles using chitosan as stabilization media [33], departing from magnetite/chitosan composites. To our knowledge, there is no report on the preparation of core/shell magnetic nanoparticles using chitosan biopolymer as template.

In the present work, the synthesis and characterization of magnetite/silver core/shell nanoparticles within a low molecular weight chitosan matrix is reported. The synthesis was performed by a two step procedure that involves the precipitation of magnetite nanoparticles from coordination compounds between ferric and ferrous ions with chitosan and subsequent reduction reaction of silver ions onto magnetite nanoparticles surface and within chitosan matrix. This preparation method permits to obtain highly loaded chitosan nanocomposites with small magnetite/silver core-shell nanoparticle sizes.

2. Experimental

All the substances were acquired as reactive grade from Aldrich Co. Chitosan was a low molecular weight with a degree of deacetylation of 84.5% and molecular weight of 50–190 kDa.

As a first step, hexahydrated ferric and tetrahydrated ferrous chlorides were dissolved in formic acid (88%) in order to obtain a dissolution with the stoichiometric ratio 2:1 of Fe(III):Fe(II) and concentration 34.0 mM of inorganic salts. Then, it was mixed with a previously formed dissolution of low molecular weight chitosan in formic acid at concentration of 10.0 mg/mL. The amount of each dissolution was added in the necessary proportions to obtain magnetite:chitosan weight ratio of 1:1. The resultant dissolution was placed in a Petri dish and the dissolvent was evaporated in a high vacuum chamber at room temperature. The resulting yellowish polymeric films were immersed into a NaOH aqueous dissolution with concentration of 5.0 M, resulting in a change of color to a dark-brownish indicating precipitation of iron oxide phase. The sample was then washed several times with de-ionized water in order to eliminate any traces of NaOH and finally dried at room temperature. The dried composite was dispersed in formic acid to obtain a stock colloidal suspension of stabilized iron oxide nanoparticles in chitosan.

The silver shell was produced in the second step, which was performed following two different protocols, in order to obtain magnetite:silver weight ratio of 1:1:

1. Preparation of an aqueous dissolution of silver nitrate ($AgNO_3$) that was mixed with the magnetite suspension under vigorous stirring. Silver ions were reduced by the addition of sodium bisulfate aqueous dissolution. The resulting sample of this step is namely M/SM1.

2. Preparation of an aqueous dissolution of silver nitrate ($AgNO_3$) that was incorporated to the magnetite suspension under strong stirring, followed by the dissolvent evaporation under high vacuum condition, and finally a solid state reduction reaction of silver ions within chitosan film. The resulting sample is namely M/SM2.

The crystalline and morphological characteristics of the non-coated magnetite and magnetite/silver core/shell particles was analyzed using dispersed powdered samples in acetone, by high resolution transmission electron microscopy (HRTEM) and nano-beam diffraction probe (NBD) in a JEM-2010F. High resolution images were obtained at optimum (Scherzer) focus. The magnetic characteristics of both kind of particles were analyzed by magnetization temperature dependent measures, $M(T)$, at constant magnetic field of 10 mT in the temperature range of 1.8–300 K, using a Quantum Design MPMS-5 superconducting quantum interference device (SQUID) magnetometer.

3. Results and discussion

3.1. Crystalline and morphological characterization

In order to observe the crystalline and morphological characteristics of the non-coated and silver-coated magnetite nano-particles, we proceed to analyze the obtained composites materials with HRTEM technique, whose results are shown in Fig. 1 and can be interpreted as follow. The Fig. 1a shows a non-coated magnetite nanoparticle with a diameter of 17 nm, where it is noticeable a regular crystalline arrangement of atomic sites. From that image it was obtained the Fourier transform filtered image of the indicated zone, which is displayed in the Fig. 1b. As is shown, the interplanar space is consistent with the corresponding space between planes of the family {222} from the crystalline structure of the spinel magnetite (see JCPDS 19-0629 diffraction card). Moreover, the Fourier transform image (see inset of Fig. 2b) confirms the symmetry of the particle, and suggest that its orientation with respect to the electron beam corresponds to [−1−12] crystalline direction.

The Fig. 1c shows a high-resolution image from sample M/SM1. The morphology of these particles is consistent with the reported core/shell configuration [6,10,34]. Fig. 1d shows the resulting Fourier transform filtered image taken from a selected nanoparticle of the Fig. 1c. The interplanar space is consistent with those corresponding to the space between planes of the family {311} (see JCPDS 19-0629 diffraction card), and with the silver family planes {111} (see JCPDS 4-0783 diffraction card). The comparison between the measured and reported interplanar spacing is shown in the Table 1.

The Fig. 1e shows a nanoparticle from the sample M/SM2. As it is noticeable, the core/shell structure is not clearly observed. However, the Fourier transform filtered image displayed in Fig. 1f shows a difference on the atomic sites arrangement from the center to the edge of the particle. The measured interplanar space indicates that the spacing between atomic sites at the center of particle could be attributed to family planes {220}, {311} and {222} of magnetite spinel structure, whereas towards the particle edges, the interplanar space is in correspondence with the {111} planes of the face-centered cubic structure of silver nanocrystals (see Table 1). Nevertheless, in spite of these results, it is not possible to assure that particles from sample M/SM2 show core/shell structure. Therefore, in order to clarify such composition, the crystalline characteristic was evaluated using the electron diffraction technique.
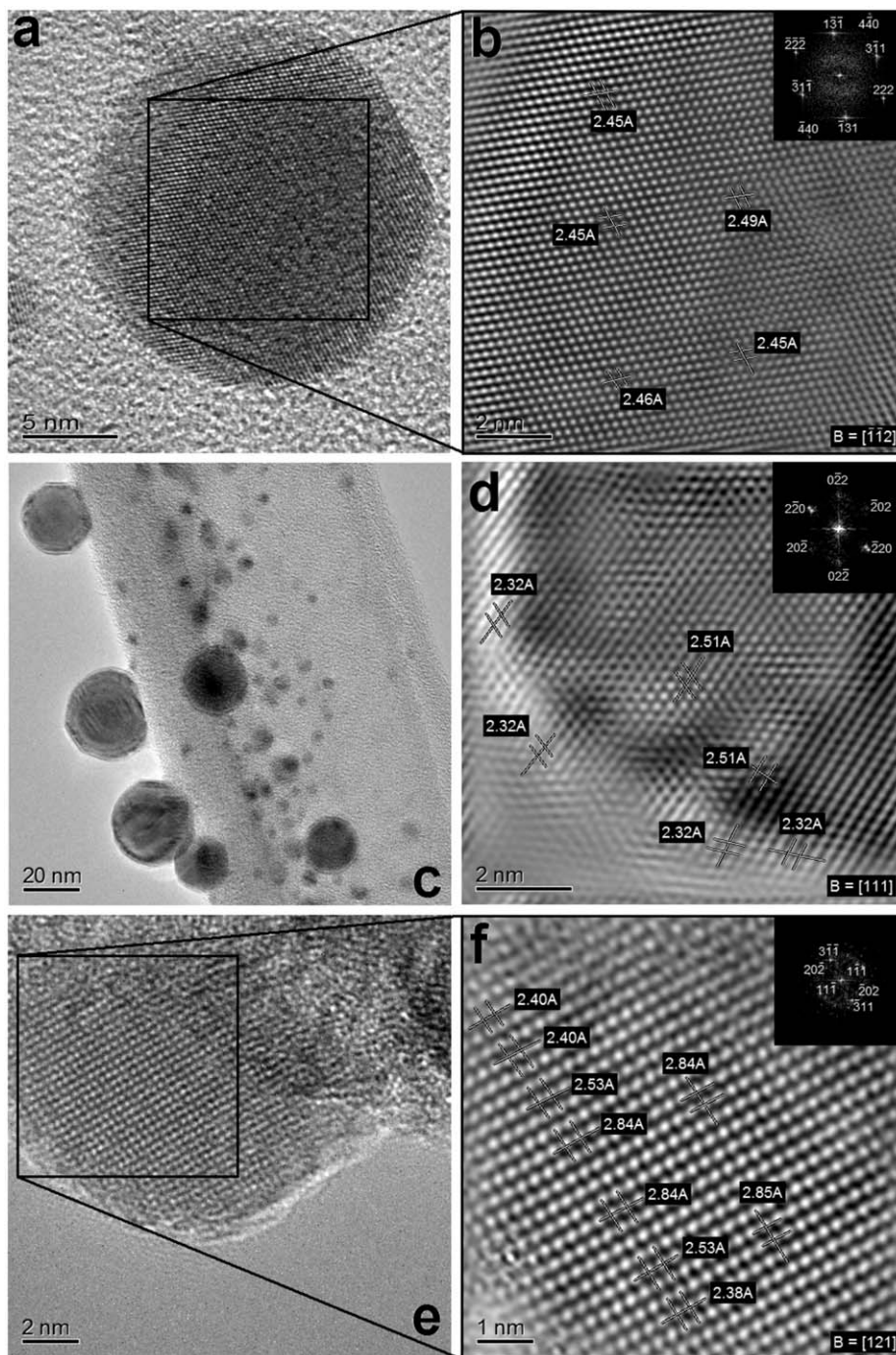
Fig. 1. Micrograph of non-coated and silver-coated magnetite samples, showing: (a) non-coated magnetite nanoparticle, (b) Fourier transform filtered image taken from the indicated selected zone, (c) nanoparticles from the sample M/SM1, (d) filtered image from a selected zone of (c), (e) nanoparticle of the sample M/SM2 and (f) Fourier transform filtered image taken from the indicated selected zone in (e). The insets in all figures show the indexed Fourier transform pattern. The value of B in all figures indicates the crystalline direction at which the electron beam is parallel.

The electron diffraction patterns obtained from samples M/SM1 and M/SM2 are shown in Fig. 2. The Fig. 2a displays the corresponding pattern taken from a nanoparticle of sample M/SM1. There, it is noticeable the presence of reflecting planes of both magnetite and silver crystalline structure. Moreover, as the Fig. 2b shows there are reflections associated to both crystalline arrangements, suggesting that particles from sample M/SM2 could also present core/shell structure with magnetite core and silver shell. The calculated interplanar distances of each indexed spot are depicted and compared with the reported for magnetite and silver crystalline structures in Table 1.

3.2. Magnetic properties

The magnetic characteristics of the synthesized non-coated and silver-coated magnetite nanoparticles systems were analyzed by magnetization temperature dependent, $M(T)$, measures. The Fig. 3 shows the zero field-cooled (ZFC) and field-cooled (FC) $M(T)$ curves obtained from non-coated magnetite nanoparticles. It is noticeable that, the $M(T)$ curves do not depict either the typical irreversibility between ZFC and FC measure nor the maximum at ZFC curve, being both related to the glassy response of single-domain magnetic nanoparticles as has been reported in the
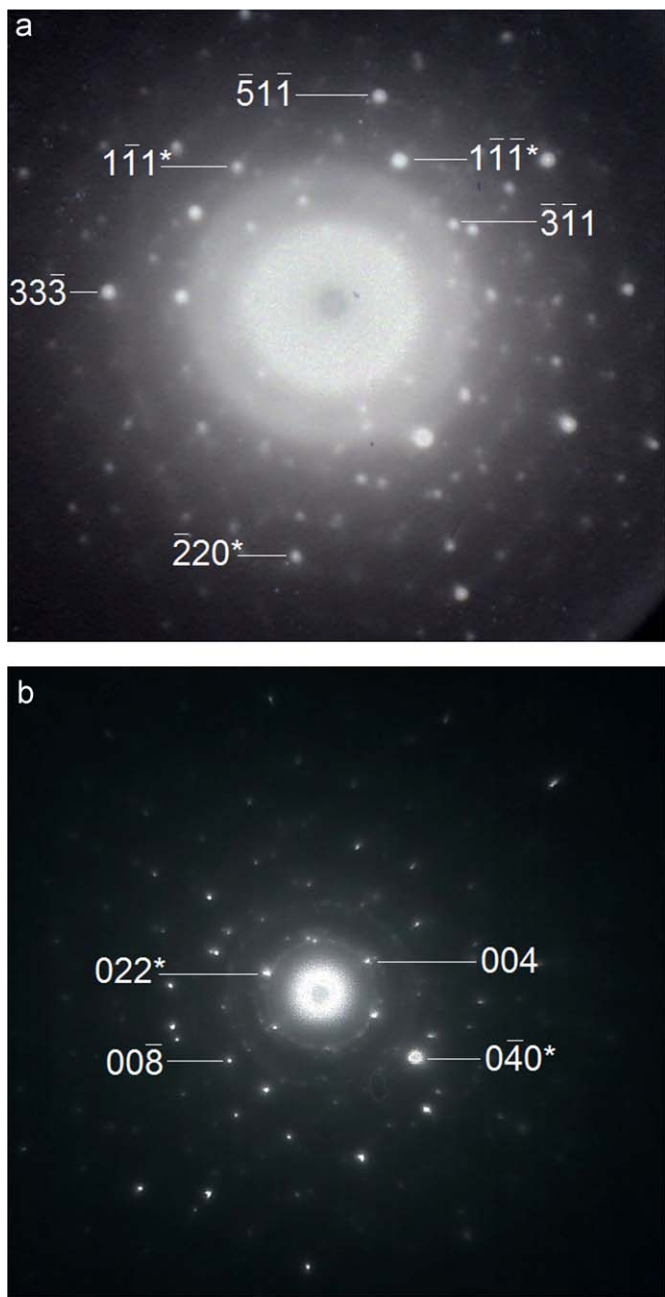
Fig. 2. Selected area electron diffraction performed to (a) M/SM1 and (b) M/SM2 samples, using NBD nano-probe. Indexed planes indicated with a star correspond to silver crystalline planes.

Table 1
Comparison of the reported interplanar spacing of both magnetite core and silver shell with the experimental measurements.

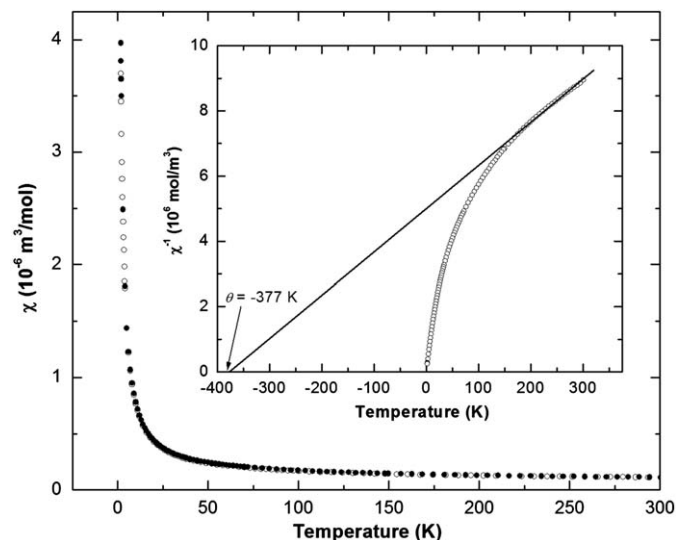| Interplanar spacing (Å)				Miller indices	
Reported		Experimental			
Fe_3O_4[a]	Ag[b]	d_{hkl}[c]	d_{hkl}[d]	Fe_3O_4	Ag
2.97	–	2.84[e]	–	(220)	–
2.53	–	2.51[f]	2.50[e]	(311)	–
2.42	–	2.40[f]	–	(222)	–
–	2.36	2.32[e]	2.30[e]	–	(111)
2.10	–	–	2.09[f]	(400)	–
1.62	–	–	1.66[e]	(511)	–
–	1.45	–	1.41[e]	–	(220)
1.42	–	–	1.42[f]	(531)	–
1.05	–	–	1.05[f]	(800)	–
–	1.02	–	1.03[e]	–	(400)

[a] JCPDS 19-0629 Diff. card.
[b] JCPDS 4-0783 Diff. card.
[c] HRTEM imaging.
[d] Electron diffraction patterns.
[e] Sample M/SM2.
[f] Sample M/SM1.

Fig. 3. Zero field-cooled (open circles) and field cooled (filled circles) $M(T)$ curves obtained from non-coated magnetite nanoparticles system. Inset show the fitting of the Curie–Weiss law (solid line) and the experimental inverse susceptibility data points.

literature [35,36]. Instead, the $M(T)$ curves displayed a Curie–Weiss behavior, which could be attributed to the response of ferrimagnetic ordered spin magnetic moments, and is given by [37]

$$\chi = \frac{C_m}{T - \theta} \qquad (1)$$

where θ is the Curie–Weiss temperature and C_m is the Curie molar constant, which can be expressed as

$$C_m = \frac{2xN_A\mu_0\mu_{eff}^2}{3k_B} \qquad (2)$$

Here, x represents the stoichiometric amounts of ions that contribute with its spin magnetic moment to the magnetic response per formula unit, k_B is the Boltzmann's constant, N_A is

the Avogadro's number, μ_0 the permeability of free space ($4\pi \times 10^{-7}$ Wb/A-m) and μ_{eff} is the effective magnetic moment.

However, as the inset in the Fig. 3 shows, the evolution of the inverse susceptibility in temperature does not depict typical hyperbolic feature as ferrimagnetic ordering does, which intersects the positive temperature axis [37]. As it is well known, the ferrimagnetic ordering is defined as the uncompensated antiferromagnetic coupling between two sublattices where divalent and trivalent metal ions founds distributed. In such case, the observed hyperbolic behavior in the ferrimagnetic ordered materials indicates the existence of a compensation temperature below the Curie point, at which the two sublattices have equal magnetic moment, resulting in net magnetic moment of zero [37,38]. In spite of that, from our measures is clear that the inverse susceptibility curve tends to intersect the temperature axis at zero, suggesting the absence of

interactions between magnetic moments associated to each magnetite nanoparticle.

Nevertheless, the high temperature behavior of the inverse susceptibility curve observed in Fig. 3 is in quite well agreement with that depicted by Eq. (1), giving values of $\theta = -377$ K and $C_m = 7.54 \times 10^{-5}$ m^3 K/mol from its fitting to the experimental results. The negative value of θ suggest that $M(T)$ response of the magnetite nanoparticles system is partially leaded by antiferromagnetic coupling between its spin magnetic moments, which theoretically overcome at $T > \theta$. However, since the $M(T)$ behavior do not show any positive to negative slope change attributed to a Néel transition [37], it is safe to say that the antiferromagnetic coupling does not extends to the entire volume of the composite, being more related to short range interactions. This kind of magnetic response is similar to that reported for diluted magnets such as magnetic-doped semiconductors, also known as diluted magnetic semiconductor (DMS), being the origin of its magnetic character related to the localized coupling between spin magnetic moments of metal ions dissolved into a semiconductor matrix [39,40]. However, is worth to emphasize that although the magnetic system of non-coated magnetite nanoparticles depicts a similar behavior, it differs from the origin of its response, which in this case could be related to the dilution of the magnetic ordering due to the dispersion of the magnetite particles into the chitosan matrix.

Using Eq. (2) is possible to calculate effective magnetic moment related to the magnetic response of the nanoparticle system. Hence, evaluating that equation with the correspondent constants values, taking $x = 1$ for magnetite and using the C_m magnitude obtained from Curie–Weiss law fitting, we calculate $\mu_{eff} = 4.9\,\mu_B$. This value is close to the reported magnetite effective moment, which is 4.1 μ_B per formula unit [38], showing that the observed magnetic response in non-coated particles system is due to the diluted or localized coupling between magnetite particles.

The Fig. 4 shows the ZFC and FC obtained from $M(T)$ measures to the sample M/SM1. As this figure shows, the $M(T)$ curves describe a Curie–Weiss behavior, similar to the non-coated sample. Nevertheless, low temperature irreversibility between ZFC and FC is observed, which displays a susceptibility increase for FC above that observed in ZFC. This behavior could be attributed to the presence of the silver shell onto magnetite nanoparticles, reducing the localized antiferromagnetic coupling

between particles magnetic moment. This is corroborated by the adjust of the experimental inverse susceptibility data to Curie–Weiss law, where it is clearly observed a reduction of the value of θ from -377 to -252 K. Furthermore, a noticeable reduction of the susceptibility with respect to the obtained from non-coated magnetite sample is observed (see Fig. 3). Such behavior suggests that also the long-range magnetic ordering of magnetite nanoparticles assembly is affected by the imposed non-magnetic silver shell. The influence of the silver shell over the magnetic response of magnetite nanoparticles assemblies has been reported previously for similar systems obtained by different synthetic routes [19,20].

4. Conclusions

Following the synthesis routes established in this paper, it was possible to elaborate magnetite and magnetite/silver core/shell nanoparticles within chitosan matrix, which depict a diluted magnet behavior attributed to the dispersion of the magnetic nanoparticles into the chitosan matrix. As the $M(T)$ curves shows, the silver shell modify the behavior of the nanoparticles system, diminishing both localized antiferromagnetic coupling and long-range particles magnetic ordering. It is important to mention that this diluted magnetic character has not been reported previously for any polymer/metal-oxide system. Therefore the experimental approach reported in this work represents a substantial contribution on the study of the magnetic properties of advance and nanoscaled materials.

Supplementary data

Supplementary data provides low magnification TEM images of both magnetite/silver core/shell samples, M/SM1 and M/SM2, in order to show that the suggested synthesis route gives remarkable particle dispersion, into the chitosan matrix, and good homogeneity on their sizes and shape.

Appendix A. Supplementary material

Supplementary data associated with this article can be found in the online version at doi:10.1016/j.jssc.2009.10.019.

Fig. 4. Zero field-cooled (open circles) and field cooled (filled circles) $M(T)$ curves obtained from the sample M/SM1. Inset shows the fitting of the Curie–Weiss law (solid line) and the experimental inverse susceptibility data points.

References

[1] M. Azad Malik, P. O'Brien, N. Revaprasadu, Chem. Mater. 14 (2002) 2004–2010.
[2] P. Reiss, J. Bleuse, A. Pron, Nano Lett. 2 (2002) 781–784.
[3] M. Mikhaylova, D. Kyung Kim, N. Bobrysheva, M. Osmolowsky, V. Semenov, T. Tsakalakos, M. Muhammed, Langmuir 20 (2004) 2472–2477.
[4] A. Hutten, D. Sudfeld, I. Ennen, G. Reiss, W. Hachmann, U. Heinzmann, K. Wojczykowski, P. Juntzi, W. Saikaly, G. Thomas, J. Biotech. 112 (2004) 47–63.
[5] Z. Huang, F. Tang, J. Colloid Inter. Sci. 275 (2004) 142–147.
[6] S. Cho, J. Idrobo, J. Olamit, K. Liu, N.D. Browning, S.M. Kauzlarich, Chem. Mater. 17 (2005) 3181–3186.
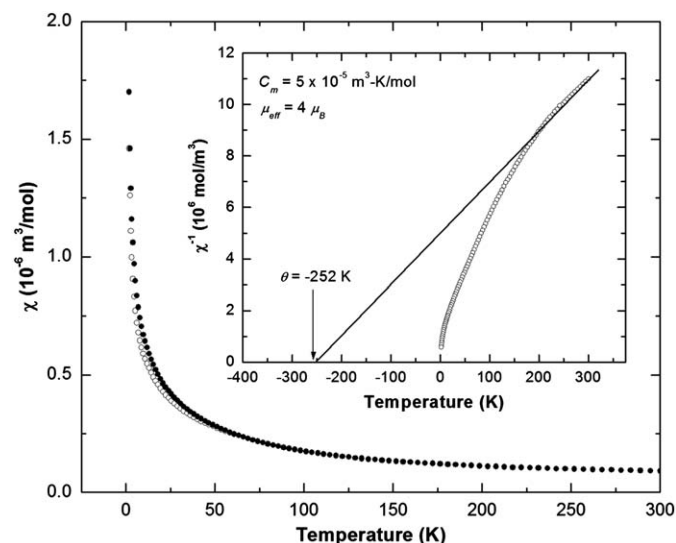[7] R. Asmatulu, M.A. Zalich, R.O. Claus, J.S. Riffle, J. Magn. Magn. Mater. 29 (2005) 108–119.

[8] Q.A. Pankhurst, J. Connolly, S.K. Jones, J. Dobson, J. Phys. D. Appl. Phys. 36 (2003) 167–181.
[9] M. Yamaura, R.L. Camilo, M.C.F.C. Felinto, J. Alloys Compds. 344 (2002) 152–156.
[10] E.E. Carpenter, S. Calvin, R.M. Stroud, V.G. Harris, Chem. Mater. 15 (2003) 3245–3246.
[11] H. Zeng, J. Li, Z.L. Wang, J.P. Liu, S. Sun, Nano Lett. 4 (2004) 187–190.
[12] H. Zeng, S. Sun, J. Li, Z.L. Wang, J.P. Liu, Appl. Phys. Lett. 85 (2004) 792–794.
[13] L. Wang, J. Luo, Q. Fan, M. Suzuki, I.S. Suzuki, M.H. Engelhard, Y. Lin, N. Kim, J.Q. Wang, C. Zhong, J. Phys. Chem. B 109 (2005) 21593–21601.
[14] J.L. Lyon, D.A. Fleming, M.B. Stone, P. Schiffer, M.E. Williams, Nano Lett. 4 (2004) 719–723.
[15] G. Salazar-Alvarez, J. Sort, S. Suriñach, M.D. Baró, J. Nogués, J. Am. Chem. Soc. 129 (2007) 9102–9108.
[16] J. Nogués, V. Skumryev, J. Sort, S. Stoyanov, D. Givord, Phys. Rev. Lett. 97 (2006) 157203.
[17] O. Masala, R. Seshadri, J. Am. Chem. Soc. 127 (2005) 9354–9355.
[18] C. Lai, T. Wu, M. Lan, IEEE Trans. Magn. 41 (2005) 3397–3399.
[19] M. Mandal, S. Kundu, S.K. Ghosh, S. Panigrahi, T.K. Sau, S.M. Yusuf, T. Pal, J. Colloid Interface Sci. 286 (2005) 187–194.
[20] E. Iglesias-Silva, J. Rivas, L.M. León-Isidro, M.A. López-Quintela, J. Non-Cryst. Solids 353 (2007) 829–831.
[21] K. Donadel, M.D.V. Felisberto, V.T. Fávere, M. Rigoni, N.J. Batistela, M.C.M. Laranjeira, Mater. Sci. Eng. C 28 (2008) 509–514.
[22] E. Onsoyen, O. Skaugrud, J. Chem. Technol. Biotechnol. 49 (1990) 345–404.
[23] J.R. Deans, B.G. Dixon, Water Res. 26 (1992) 469–472.
[24] G.L. Rorrer, T.-Y. Hsien, J.D. Way, Ind. Eng. Chem. Res. 32 (1993) 2170–2178.
[25] W. Kaminski, Z. Modrzejewska, Sep. Sci. Technol. 32 (1997) 2659–2668.
[26] R. Schmuhl, H.M. Krieg, K. Keizer, Water SA 27 (2001) 1–8.
[27] A. Burke, E. Yilmaz, N. Hasirci, Turk. J. Med. Sci. 30 (2000) 341–348.
[28] L. Jin, R. Bai, Langmuir 18 (2002) 9765–9770.
[29] A.K. Boal, K. Das, M. Gray, V.M. Rotello, Chem. Mater. 14 (2002) 2628–2636.
[30] H. Lee, H. Shao, Y. Huang, B. Kwak, IEEE Trans. Magn. 41 (2005) 4102–4104.
[31] H.S. Lee, E.H. Kim, H. Shao, B.K. Kwak, J. Magn. Magn. Mater. 293 (2005) 102–105.
[32] E.H. Kim, Y. Ahnb, H.S. Lee, J. Alloys Compds. 434–435 (2007) 633–636.
[33] D. Cheng, X. Zhou, H. Xia, H. Chan, Chem. Mater. 17 (2005) 3578–3581.
[34] J. Li, H. Zeng, S. Sun, J. Ping Liu, Z. Lin Wang, J. Phys. Chem. B 108 (2004) 14005–14008.
[35] D.L. Leslie-Pelecky, R.D. Rieke, Chem. Mater. 8 (1996) 1770–1783.
[36] J. Mürbe, A. Rechtenbach, J. Töpfer, Mater. Chem. Phys. 110 (2008) 426–433.
[37] M. Getzlaff, Fundamentals of Magnetism, first ed., Springer, Berlin, 2008.
[38] A. Goldman, Modern Ferrite Technology, second ed., Springer Science+Business Media, New York, 2006.
[39] J.K. Furdyna, N. Samarth, R.B. Frankel, Phys. Rev. B 37 (1988) 3707–3709.
[40] R. Cárdenas, F.V. Pérez, M. Quintero, E. Quintero, R. Tovar, M. Morocoima, J. González, P. Bocarada, J. Ruiz, J.M. Broto, H. Rakoto, Physica B 389 (2007) 302–305.